Available online at www.sciencedirect.com
ScienceDirect
Trans. Nonferrous Met. Soc. China 32(2022) 593−603
Transactions of Nonferrous Metals Society of China
www.tnmsc.cn

Regeneration of Al-doped $LiNi_{0.5}Co_{0.2}Mn_{0.3}O_2$ cathode material by simulated hydrometallurgy leachate of spent lithium-ion batteries

Fang-cheng LI[1], Gang ZHANG[2,3], Zong-liang ZHANG[1], Jian YANG[1], Fang-yang LIU[1], Ming JIA[1], Liang-xing JIANG[1]

1. School of Metallurgy and Environment, Central South University, Changsha 410083, China;
2. Zhongtian Supercapacitor Technology Co., Ltd., Nantong 226463, China;
3. Zhongtian Emerging Materials Co., Ltd., Nantong 226463, China

Received 8 February 2021; accepted 20 October 2021

Abstract: A uniform Al-doped $LiNi_{0.5}Co_{0.2}Mn_{0.3}O_2$ cathode material was prepared using a coprecipitation method to take advantage of the positive effect of Al on regenerated NCM (Ni, Co, Mn) cathode materials and ameliorate cumbersome and high-cost impurity removal processes during lithium-ion battery recycling. When the Al^{3+} content in the leachate was 1 at.% with respect to the total amount of transition metals (Ni, Co, and Mn), the produced Al-doped NCM cathode material increased concentrations of lattice oxygen and Ni^{2+}. The initial specific capacity at 0.1*C* was 167.4 mA·h/g, with a capacity retention of 79.1% after 400 cycles at 1*C*. Further, this Al-doped sample showed improved rate performance and a smaller electrochemical impedance. These findings provide a reference for developing industrial processes to resynthesize cathode materials with improved electrochemical performance by incorporating Al^{3+} impurities produced during lithium-ion battery recycling.

Key words: spent lithium-ion battery; regeneration; Al doping; ternary cathode material; coprecipitation

1 Introduction

With the development of society, lithium-ion batteries (LIBs) have become increasingly popular in consumer electronics, electric vehicles, large-scale energy storage, and other fields owing to their high energy density, long cycle life, low self-discharge rate, and nonexistent memory effect [1−3]. Owing to their widespread use and limited lifespan, a considerable number of spent LIBs have been produced [4−6]. LIBs contain numerous valuable metals, such as Li, Ni, Co, Mn, Al, and Cu, as well as a variety of toxic organic substances, such as electrolytes, separators, and binders [7−9]. Therefore, recycling spent LIBs is not only economically beneficial but also can reduce environmental pollution and promote green and sustainable development.

In general, the industrial disposal of spent LIBs is achieved using a combination of pyro-pretreatment and hydrometallurgical extraction [10−13]. In the pretreatment process, the discharged battery is disassembled, separated, and calcined at high temperatures. The powdered cathode material usually contains a small number of fine particles from the Al foil cathode collector, which, following the subsequent leaching process, exist in the leachate in the form of Al^{3+} [14,15]. After purification, the leachate can be utilized either to produce a single metal salt or to directly resynthesize an NCM (Ni, Co, Mn) precursor after adjusting the composition of the purified solution [16,17].

We previously reported a simple and efficient method for recovering Li, Ni, Co, and Mn from spent LIB cathode materials [16,18]. This two-stage countercurrent leaching method improved the metal leaching rate and the acid utilization rate. In

Corresponding author: Liang-xing JIANG, Tel: +86-15116335788, E-mail: lxjiang@csu.edu.cn
DOI: 10.1016/S1003-6326(22)65818-7

addition to the above four metals, the leachate also contained Al^{3+} impurities. Al^{3+} doping in NCM layered cathode materials has become a research hotspot because it can improve the electrochemical performance and reduce the thermal instability [15,19,20]. Therefore, if the concentration of Al^{3+} in the leachate obtained by recycling spent LIBs is appropriately controlled, the purified Al-containing leachate can be used to prepare Al-doped NCM layered cathode materials with good electrochemical performance and thermal stability. In this study, the influence of the Al^{3+} content in the mixed metal salt solution for precursor preparation on the morphology and electrochemical performance of the final layered cathode material was systematically investigated. The determined optimal doping amount provides a theoretical basis for impurity removal limits in LIB recycling processes.

2 Experimental

2.1 Synthesis of materials

Because this study required a large amount of mixed metal salt solution, the leachate produced in the laboratory could not meet the experimental requirements. Therefore, chemically pure reagents were used to prepare five different $LiNi_{0.5}Co_{0.2}Mn_{0.3}O_2$ layered cathode materials using a hydroxide coprecipitation method followed by a solid-phase sintering method. The prepared samples with Al/transition metal (TM; Ni + Co + Mn) ratios of 0, 0.1, 0.5, 1, and 2 at.% were named NCM523, A0.1, A0.5, A1, and A2, respectively.

First, a mixed metal salt solution ($NiSO_4·6H_2O$:$CoSO_4·7H_2O$:$MnSO_4·H_2O$ = 5:2:3, molar ratio) with a total concentration of 2 mol/L and a mixed alkali solution with 4.2 mol/L NaOH and 0.6 mol/L $NH_3·H_2O$ were prepared with deionized water. Further, 0.3 mol/L $NH_3·H_2O$ was prepared as the bottom solution in the reaction kettle. $Al_2(SO_4)_3·18H_2O$, which was used as the Al source, was added to the mixed metal salt solution at the required concentration. The mixed metal salt solution and mixed alkali solution were pumped into a 5 L continuously stirred reaction kettle and then aged for more than 16 h. The temperature of the reactor was maintained at 50 °C during the test, and the pH was maintained at 11.1 by controlling the feeding speed of the mixed alkali solution. Subsequently, obtained precursor was rinsed with deionized water, filtered, and dried under vacuum at 105 °C for 15 h. The $Ni_{0.5}Co_{0.2}Mn_{0.3}(OH)_2$ precursor and Li_2CO_3 were mixed well at a Li/TM molar ratio of 1.05:1 and then roasted using a two-stage roasting method (first heating to 500 °C for 5 h and then to 850 °C for 15 h). Finally, the Al-doped $LiNi_{0.5}Co_{0.2}Mn_{0.3}O_2$ cathode material was obtained.

2.2 Material characterization

The morphological characteristics and elemental distributions of the materials were analyzed using field-emission scanning electron microscopy (SEM; JSM−7900F) coupled with energy-dispersive X-ray spectroscopy (EDAX Octane). X-ray diffraction (XRD; Advance D8) data were collected in the 2θ range of 10°−80° at a sweep speed of 0.1 (°)/s. Inductively coupled plasma optical emission spectrometry (ICP-OES; Spectro Blue SOP) was used to determine the elemental compositions of the precursor materials. The oxidation states of the elements on the material surfaces were determined using X-ray photoelectron spectroscopy (XPS; ESCALAB 250Xi).

2.3 Electrochemical tests

Electrochemical tests were carried out using CR-2025-type coin cells. A slurry was fabricated by dispersing a mixture of 80 wt.% active material, 10 wt.% acetylene black as a conducting material, and 10 wt.% polyvinylidene fluoride as a binder in *N*-methyl-2-pyrrolidone. To prepare the test electrode, the slurry was coated on Al foil and dried at 80 °C for 12 h. A lithium metal sheet was used as the counter electrode and Celgard 2400 was used as the separator. The electrolyte was 1 mol/L lithium hexafluorophosphate ($LiPF_6$) in a mixture of ethylene carbonate, diethyl carbonate, and ethyl methyl carbonate (1:1:1, volume ratio). Fresh coin cells were assembled in a dry Ar-filled glove box. Galvanostatic charge–discharge tests were performed using a LAND battery-testing instrument. Coin cells were tested at 25 °C in a voltage range of 2.8−4.3 V (vs Li/Li^+). Cyclic voltammetry (CV) measurements were conducted using a CHI 660E electrochemical workstation at a scan rate of 0.1 mV/s. Electrochemical impedance spectroscopy measurements were performed on a PARSTAT 4000A electrochemical workstation using a 10 mV

amplitude sine wave in the frequency range of 100 kHz to 0.01 Hz.

3 Results and discussion

3.1 Characterization of materials

Based on the ICP-OES results (Table 1), the elemental compositions of the as-prepared precursors were consistent with the experimental design, indicating that the Al ions were successfully doped into the precursor materials. Figure 1 shows the SEM images of the synthesized Al-doped $Ni_{0.5}Co_{0.2}Mn_{0.3}(OH)_2$ samples, which consisted of compactly packed nanoscale primary flakes and spherical secondary particles with particle sizes of 3−5 μm. The secondary particles were small and agglomerated, which may be due to an insufficient feed time in the small reactor volume [21−23]. As the Al content in the precursor increased, the thickness of the primary flakes gradually decreased, whereas the shape and size of the secondary particles remained unchanged. However, when the Al content reached 2 at.%, the primary particles were loosely packed and the secondary particles had poor sphericity. As shown by the elemental mapping results for the A1 sample in Fig. 2(a), Ni, Co, Mn, and Al were uniformly distributed on the surface of the secondary particles. Furthermore, the elemental line scanning profiles for a particle cross-section (Fig. 2(b)) reveal that the concentrations of Ni, Co, Mn, and Al were uniform throughout the secondary particles.

The XRD patterns of the prepared precursors and the corresponding cathode materials are shown in Figs. 3 and 4, respectively. As shown in Fig. 3, the XRD patterns of all the precursors corresponded to β-Ni(OH)$_2$ ($P3m1$ space group). However, for the A0.1 sample, the peaks attributed to the (001) and (101) crystal planes were shifted to larger angles by approximately 0.2°, whereas no shift was observed for the A0.5 sample. For the A1 and A2 samples, only the peak attributed to the (101) crystal face shifted to a larger angle by approximately 0.5°. Based on the Bragg equation ($\lambda=2d\sin\theta$) at a constant incident wavelength, a shift of the diffraction angle to a larger angle after doping indicates that the interplanar spacing d is reduced. As the radius of Al^{3+}(0.535 Å) is smaller than those of Ni^{2+} (0.69 Å) and Ni^{3+} (0.560 Å), Al^{3+} doping in TM sites can reduce the interplanar spacing. However, owing to the different doping amounts and the lack of control over doping sites, diffraction peak shifts were only observed for some samples. These phenomena indicate that the unit volume was decreased [24] by Al^{3+} entering the lattice sites.

After mixing with lithium carbonate and high-temperature calcination, all the cathode materials showed high crystallinity and a hexagonal α-$NaFeO_2$ layered structure ($R\bar{3}m$ space group), and no obvious impurity peaks were observed

Table 1 ICP-OES results for prepared precursor (wt.%)

Precursor	Ni	Co	Mn	Al	n_{Ni}:n_{Co}:n_{Mn}	n_{Al}:n_{TM}
A0.1	32.2	12.6	18.5	0.033	5.1323:2.0001:3.1500	0.0011:1
A0.5	31.8	12.7	18.4	0.15	5.0686:2.0160:3.1329	0.0051:1
A1	31.9	12.3	18.2	0.29	5.0845:1.9525:3.0989	0.0099:1
A2	31.6	12.4	18.1	0.57	5.0367:1.9684:3.0819	0.0196:1

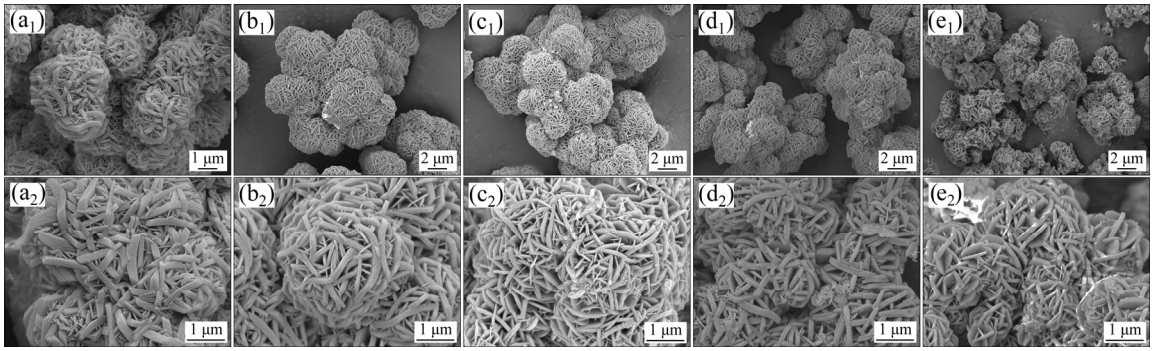

Fig. 1 SEM images of NCM523 (a_1, a_2), A0.1 (b_1, b_2), A0.5 (c_1, c_2), A1 (d_1, d_2), and A2 (e_1, e_2) precursors

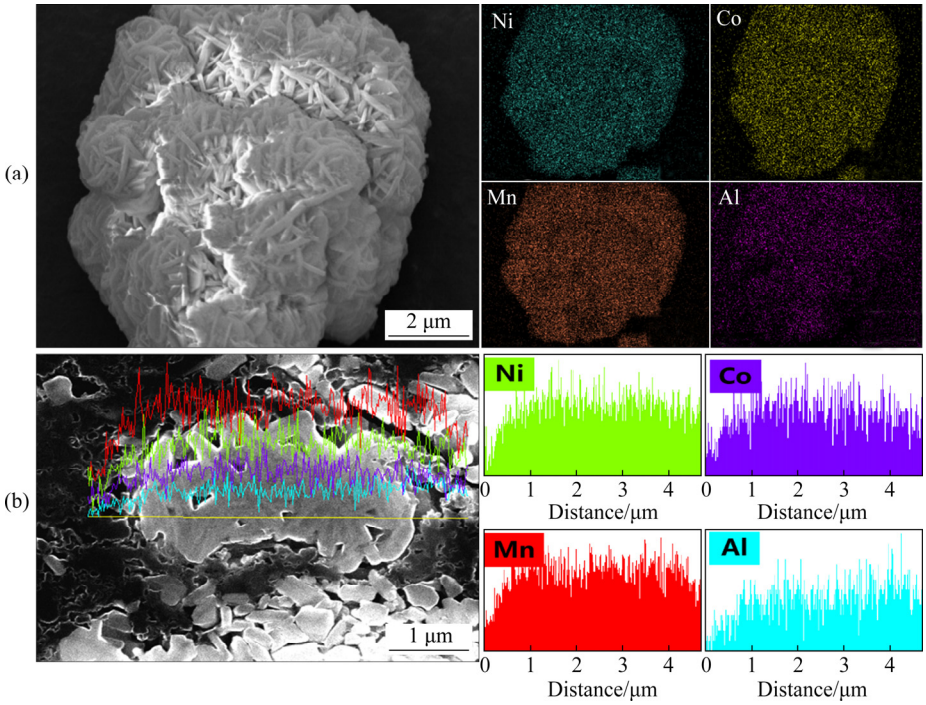

Fig. 2 Elemental mapping of Ni, Co, Mn, Al in A1 sample (a) and corresponding elemental line scanning profiles for particle cross-section (b)

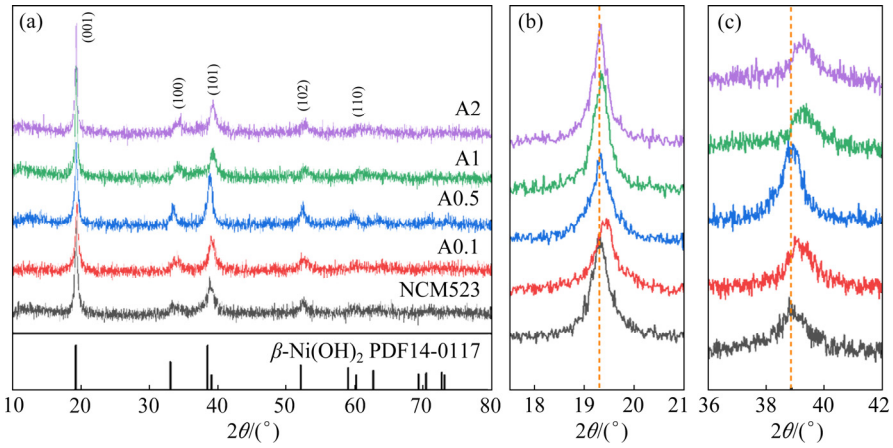

Fig. 3 XRD patterns of precursors (a) and expanded views of peaks corresponding to (001) plane (b) and (101) plane (c)

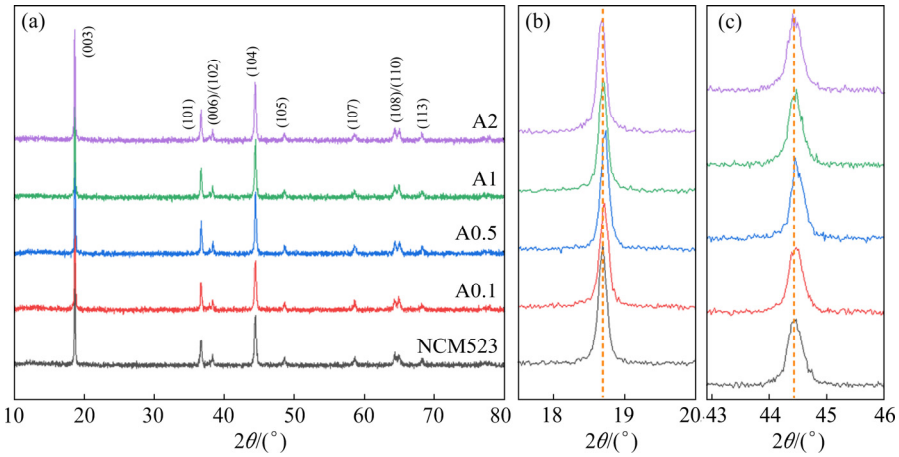

Fig. 4 XRD patterns of cathode materials (a) and expanded view of peaks corresponding to (003) plane (b) and (104) plane (c)

(Fig. 4). Further, an apparent splitting of the (006)/(102) and (108)/(110) crystal planes occurred, indicating that these materials had highly ordered layered structures [25−27]. These results indicate that a small amount of Al^{3+} doping does not change the layered structure of $LiNi_{0.5}Co_{0.2}Mn_{0.3}O_2$. It should be noted that the diffraction peak shifts observed for the precursors almost disappeared after high-temperature calcination. The lattice parameters of samples are listed in Table 2. A low degree of Li/Ni mixing was observed ($I_{(003)}/I_{(104)}$ >1.2), which is favorable for good electrochemical performance [23]. The *c*/*a* ratios were all greater than 4.9, indicating that the materials had good layered structures [28]. Importantly, as Al^{3+} doping increased, the *c*/*a* ratio gradually increased, suggesting that Al^{3+} doping enhanced the layered structure of the cathode materials.

Table 2 Lattice parameters of synthesized cathode samples

Sample	*a*/Å	*c*/Å	*V*/Å^3	*c*/*a*	$I_{(003)}/I_{(104)}$
NCM523	2.87268	14.22305	101.65	4.951	2.041
A0.1	2.87427	14.24220	101.60	4.955	1.841
A0.5	2.86951	14.24176	101.64	4.963	1.719
A1	2.87003	14.24675	101.57	4.964	1.729
A2	2.8712	14.26081	101.56	4.967	1.736

According to first-principles calculations [29], when Al^{3+} occupies the Ni^{3+} site, because the ionic radius of Al^{3+} (0.535 Å) is smaller than that of Ni^{3+} (0.560 Å), lattice parameter *a* and the thickness of the TMO_6 layer decrease [19]. In addition, because the electronegativity of Al^{3+} is smaller than that of Ni^{3+} (~1.513 and ~1.695, respectively) [30], Al^{3+} doping makes the TM—O bond more ionic. Further, the electrostatic repulsion between oxygen layers is increased because the charge density of the oxygen layers is higher. Thus, lattice parameter *c* and the thickness of the LiO_6 layer both increase after Al^{3+} doping [31].

The above considerations explain the larger *c*/*a* ratios and improved layered structures of the doped cathode materials. Further, increasing the thickness of the LiO_6 layer is expected to enhance the two-dimensional diffusion of Li^+, thus improving the cycling and rate properties of the material to a certain extent. In addition, as the bond energy of Al—O (512 kJ/mol) is greater than those of Ni—O (391.6 kJ/mol), Co—O (368 kJ/mol), and Mn—O (402 kJ/mol) [32,33], Al^{3+} doping can effectively inhibit anisotropic lattice mutations and improve the stability of the crystal structure during Li^+ deintercalation, which is favorable for enhancing the cycle performance and thermal stability [19]. In addition, it has recently been reported that Al—O bonds on the surface/subsurface inhibit chemical reactions with acidic electrolytes, thereby preventing electrolyte penetration and maintaining structural stability[34].

To further study the chemical states of the samples, XPS measurements were performed for the sintered NCM523 and A1 cathode material samples. As shown in Fig. 5(a), four main elements (O, Ni, Co, and Mn) were detected in both samples. In addition, Al was also detected on the surface of the A1 sample (Fig. 5(f)), although it was not observed in the full-scan spectrum because of its low content. As shown by the O 1s spectra in Fig. 5(b), the samples exhibited peaks at 531.4 and 529.3 eV, which corresponded to surface oxygen compounds and lattice oxygen, respectively. With 1 at.% Al^{3+} doping, the Al—O bonds significantly increased the concentration of lattice oxygen and enhanced the structural stability of the material. As shown in Fig. 5(c), two main Ni peaks were observed at 872.8 and 855.3 eV corresponding to Ni $2p_{1/2}$ and Ni $2p_{3/2}$, respectively. The Ni $2p_{3/2}$ peak was split into two peaks at binding energies of 854.7 and 855.7 eV corresponding to Ni^{2+} and Ni^{3+}, respectively. The Ni^{3+} contents of the NCM523 and A1 samples were 44.5% and 26.5%, respectively. In NCM523, NCM622, and NCM811 layered materials, Ni has two valence states: +2/+3 [35,36]. When less electronegative Al^{3+} occupies the Ni^{3+} site, the Ni^{2+} concentration in the surrounding crystal lattice will become relatively high, thus increasing the specific discharge capacity at the same cut-off voltage. As shown in Figs. 5(d) and (e), the Co 2p and Mn 2p spectra of both samples were similar. The Co $2p_{1/2}$ (794.8 eV) and Co $2p_{3/2}$ (779.8 eV) peaks as well as the Mn $2p_{1/2}$ (653.9 eV) and Mn $2p_{3/2}$ (642.3 eV) peaks indicated that both samples contained trivalent Co and tetravalent Mn [37]. In addition, the Al peaks at 72.3 eV and 67.9 eV in Fig. 5(f) corresponded to Al $2p_{1/2}$ and Al $2p_{3/2}$, respectively, confirming the existence of Al^{3+} in the doped sample. Overall, the XPS spectra of the NCM523 and A1 samples indicate that the

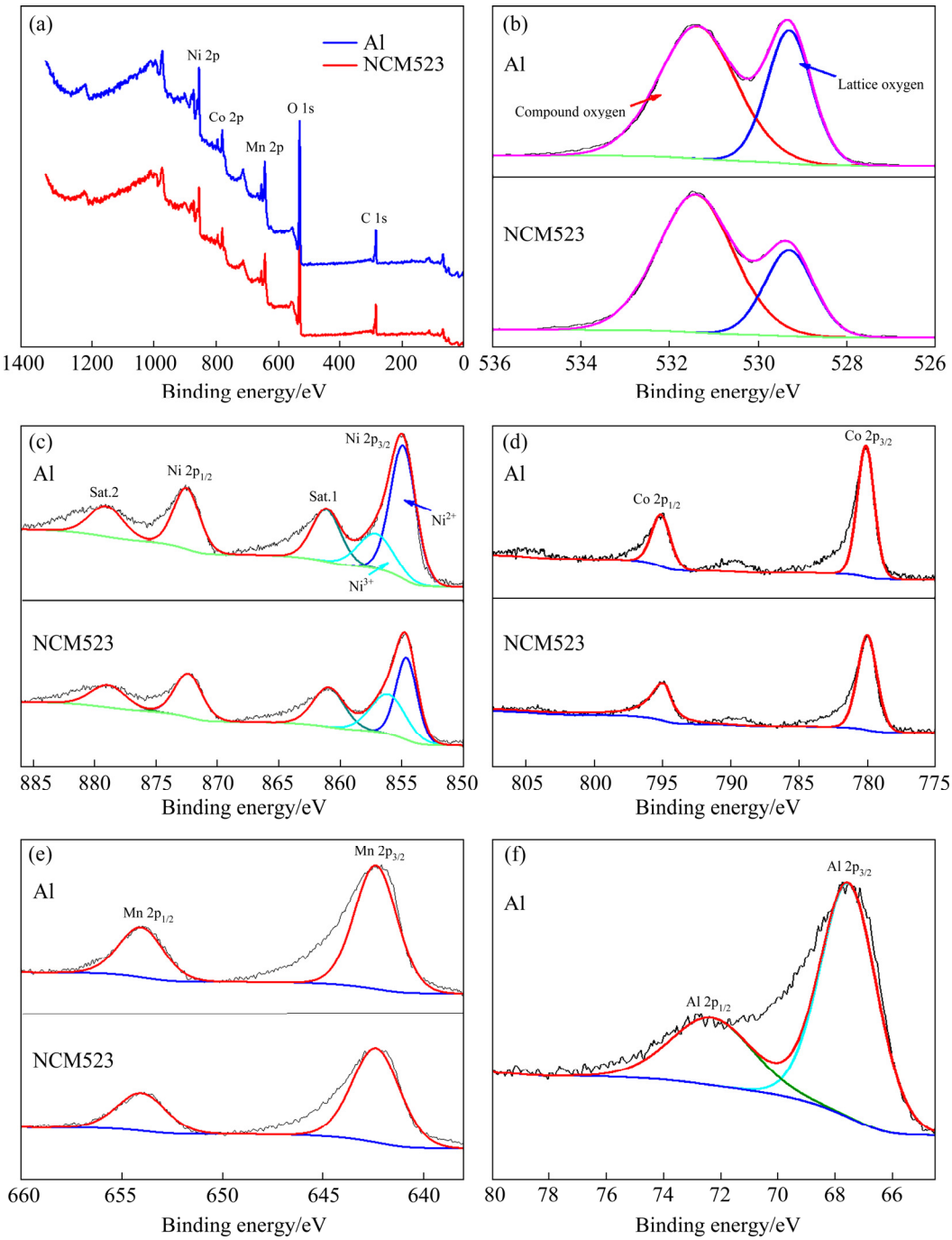

Fig. 5 Full-scan XPS spectra of NCM523 and A1 samples (a) and corresponding O 1s (b), Ni 2p (c), Co 2p (d), Mn 2p (e) and Al 2p (f) spectra

surface layer of the doped sample has a high concentration of lattice oxygen and Ni^{2+}, which enhances the structural stability and specific discharge capacity, indicating that Al^{3+} impurities in leachates can enter the crystal lattice of resynthesized precursors and cathode materials.

3.2 Electrochemical performance

To clarify the influence of Al^{3+} impurities on the electrochemical performance of the regenerated ternary materials, all materials were tested under constant current charge and discharge in the voltage window of 2.8−4.3 V (25 °C). The initial charge–discharge curves of the five cathode materials at a current density of 0.1*C* (1*C*=160 mA/g) are shown in Fig. 6(a). The initial specific charge and discharge capacities of NCM523 were 192.9 and 159.1 mA·h/g, respectively, and the coulombic efficiency was 82.51%. As Al^{3+} doping increased, the specific discharge capacity increased, with the

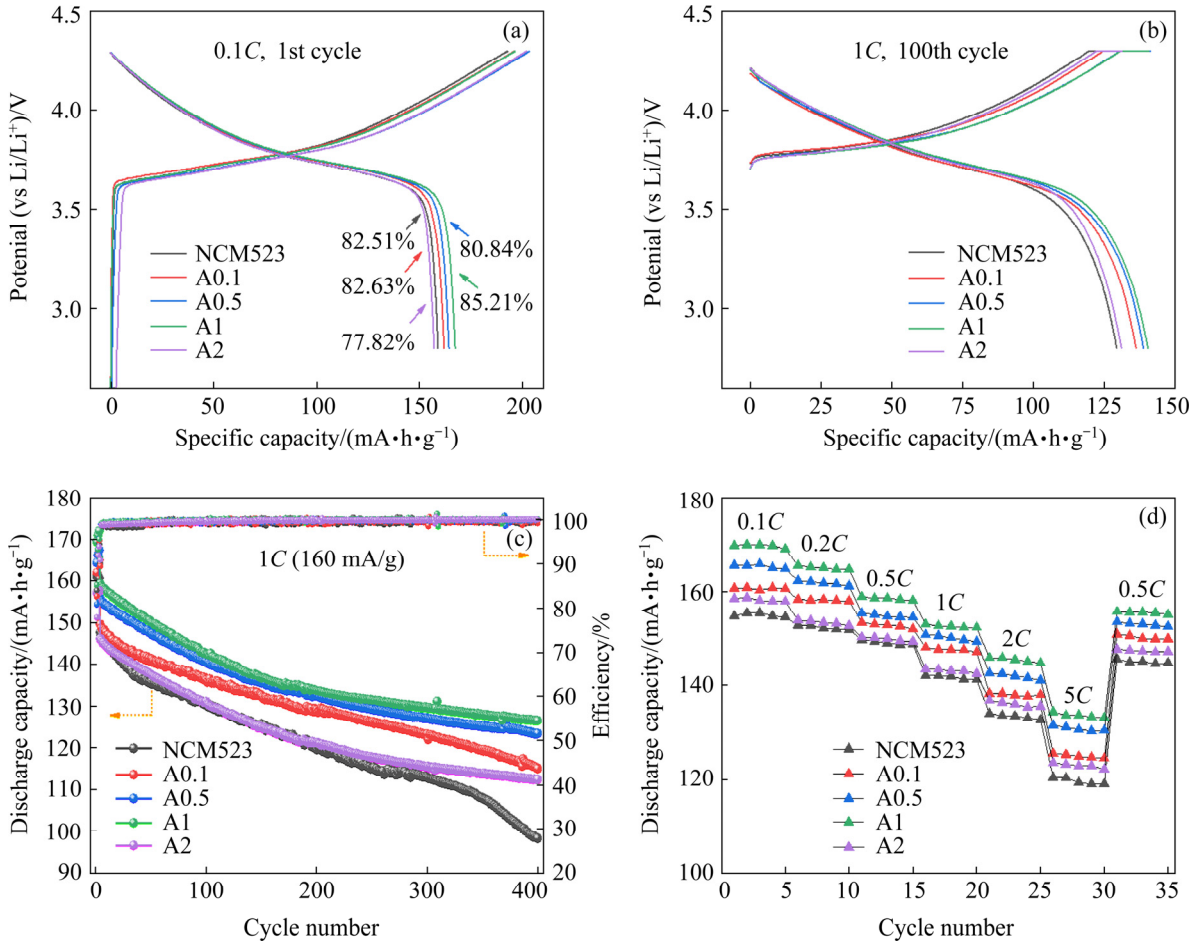

Fig. 6 Initial charge–discharge curves of cathode materials at current density of 0.1*C* (1*C*=160 mA/g) (a), charge–discharge curves after 100 cycles at 1*C* (b), cycling performance (c), and rate capability (d)

highest value of 167.4 mA·h/g obtained at 1 at.% Al^{3+}. Furthermore, this material exhibited a coulombic efficiency of 85.21%. However, when the Al^{3+} content was further increased to 2 at.%, the initial specific discharge capacity decreased to 157.2 mA·h/g, and the coulomb efficiency was only 77.82%. After 100 cycles at 1*C*, the A1 sample still had the highest specific discharge capacity, whereas the specific discharge capacity of NCM523 was the lowest (Fig. 6(b)), indicating that Al^{3+} doping can stabilize the crystal structure of the material and promote the release of Li^+.

Figures 6(c) and (d) compare the cycle and rate performance of the Al-doped samples with pristine NCM523. After 400 cycles at 1*C*, the specific discharge capacities of NCM523, A0.1, A0.5, A1, and A2 were 98.4, 115.1, 123.5, 124.6, and 112.5 mA·h/g, respectively, and the capacity retention rates were 66.6%, 76.9%, 79.3%, 79.1%, and 76.9%, respectively. Notably, the coulombic efficiencies were all greater than 99.5% after 400 cycles. In the rate test, the specific discharge capacities of NCM523 at current densities of 0.1*C*, 0.2*C*, 0.5*C*, 1*C*, 2*C*, and 5*C* were 155, 152.3, 149.1, 141.7, 133.4, and 119.6 mA·h/g, respectively. When the current density returned to 0.5*C*, the specific discharge capacity increased again to 145 mA·h/g. At the same rate, the specific discharge capacities of the A1 sample were 169.7, 165, 158.5, 152.6, 145.4, and 133.6 mA·h/g, and the capacity recovered to 155.5 mA·h/g when the rate returned to 0.5*C*. The A2 cathode material inherited the physical properties of the precursor, with loosely packed primary particles and secondary particles with poor sphericity. As a result, there were a large number of gaps on the surface of this material, which led to poor electrochemical stability at the particle–electrolyte interface. Further, the content of nonelectrochemically active Al^{3+} in the A2 sample was higher, which led to a decrease in the reversible specific capacity at the same cut-off voltage, although it was still higher than that of pristine

NCM523 prepared under the same conditions.

In summary, at a doping amount of 1 at.%, Al^{3+} greatly improved the structural stability of the cathode material, and Al—O bonds with stronger bond energies alleviated lattice changes during long-term cycling. Compared with other work in this field [15], a higher optimal doping amount and a higher specific discharge capacity at 5*C* were obtained in this study. The subsequent increase in the thickness of the LiO_6 layer was also beneficial to the two-dimensional diffusion of Li^+, which further contributed to improving the electrochemical properties.

The morphologies of the cathode materials were characterized after 400 cycles. As shown in Fig. 7(a), after 400 cycles at 1*C*, the particles in the A1 sample remained relatively complete. In contrast, a certain extent of structural collapse was observed for NCM523 (Fig. 7(b)), which further confirmed that the Al-doped cathode material had a more stable structure and better cycling stability.

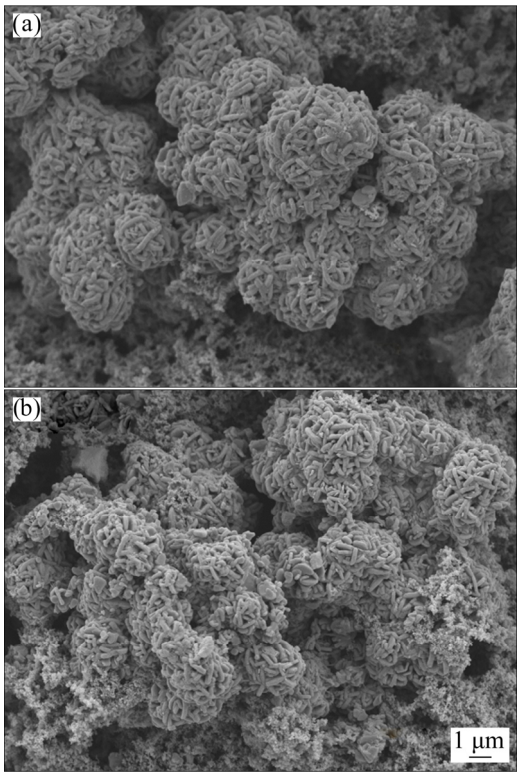

Fig. 7 SEM images of A1 (a) and NCM523 (b) samples after 400 cycles at 1*C*

To gain further insights into the origin of the enhanced electrochemical performance observed after Al^{3+} doping from the perspective of electrode polarization, CV measurements were performed for the NCM523 and A1 samples in a voltage range of 2.8−4.5 V at a scan rate of 0.1 mV/s. As shown in Figs. 8(a) and (b), only one redox peak couple was observed, which was ascribed to the Ni^{2+}/Ni^{4+} redox reaction [38]. During the first three cycles, the oxidation peak potential of NCM523 shifted from 3.831 to 3.773 V owing to the activation of the cathode material surface during the initial charge and discharge processes [39], whereas good coincidence was maintained in subsequent cycles. The oxidation peak of A1 sample initially shifted from 3.825 to 3.768 V, and excellent coincidence was the second cycle, which confirmed that doping with 1 at.% of Al^{3+} increased the reversibility of the electrode reaction. As the peak potential differences during the third circle for pristine NCM523 and A1 samples were 70 and 58 mV, respectively, doping with 1 at.% Al^{3+} decreased the electrode polarization. Further, the A1 sample exhibited a sharper peak shape than pristine NCM523, indicating that the Li^+ deintercalation kinetics was

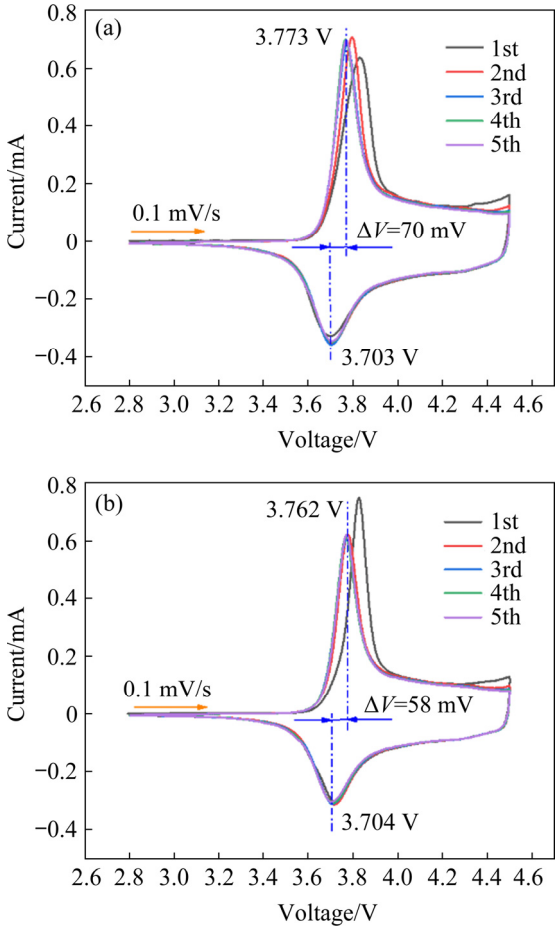

Fig. 8 Cyclic voltammograms of NCM523 (a) and A1 samples (b) in voltage window of 2.8−4.5 V at scan rate of 0.1 mV/s

improved, which also confirmed that the rate performance of the doped sample was better than that of pristine NCM523.

Figure 9 shows the electrochemical impedance spectra of the NCM523 and A1 samples after 100 cycles at 1*C*. The data were fitted to the equivalent circuit diagram shown in Fig. 9(a) to obtain the impedance parameters, where R_b represents the electrolyte impedance in the high-frequency region, R_{sf} represents the impedance of the solid electrolyte interphase film in the intermediate frequency region, R_{ct} represents the charge-transfer impedance, and W is the Warburg impedance for the diffusion of Li^+ inside the active material particles [40,41]. As shown in Table 3, after 100 cycles, the R_b, R_{sf}, and R_{ct} values of the A1 sample were 5.772, 32.08, and 218.9 Ω, respectively, whereas those for pristine NCM523 were 6.671, 18.42, and 346.3 Ω, respectively. Owing to the increase in lattice parameter *c* and the stability of the Al—O bonds, the migration performance of Li^+ was improved, thereby greatly reducing the R_{ct} value.

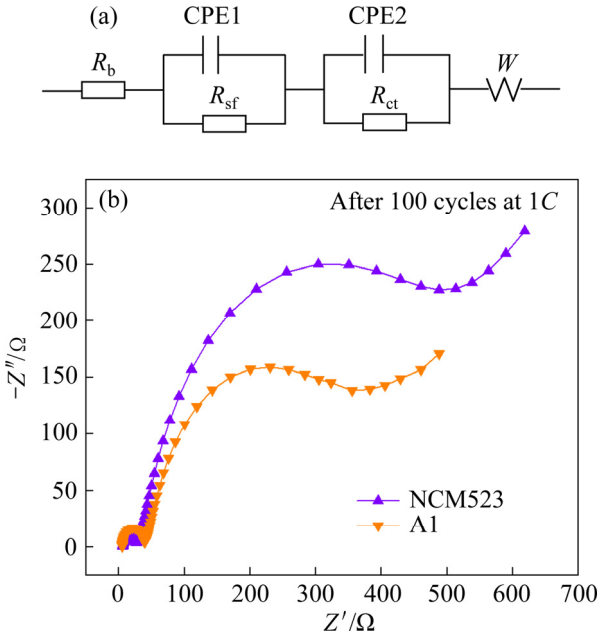

Fig. 9 Equivalent circuit (a) and electrochemical impedance spectra (b) of NCM523 and A1 samples after 100 cycles at 1*C*

Table 3 Impedance parameters for pristine NCM523 and A1 samples obtained by fitting to equivalent circuit

Sample	R_b/Ω	R_{sf}/Ω	R_{ct}/Ω
NCM523	6.671	18.42	346.3
A1	5.772	32.08	218.9

4 Conclusions

(1) Owing to continuous high-speed stirring in the reactor, Al was uniformly distributed in the cathode materials, the cathode material exhibited enhanced crystal structure stability, and the two-dimensional diffusion kinetics of Li^+ was improved.

(2) When the Al^{3+} doping content in the NCM523 cathode material was 1 at.%, the capacity retention rate after 400 cycles at 1*C* increased from 66.6% to 79.1%. Further, doping also resulted in a higher reversible capacity and a lower electrochemical impedance.

(3) This work confirmed that the Al^{3+} impurities produced during LIB recycling processes can improve the electrochemical performance of ternary cathode materials. The obtained optimal Al^{3+} doping amount of 1 at.% can provide a reference for the industrial resynthesis of LIB cathode materials.

Acknowledgments

This work was supported by Anhui Province Research and Development Innovation Project for Automotive Power Battery Efficient Recycling System, China.

References

[1] ANDRE D, KIM S J, LAMP P, LUX S F, MAGLIA F, PASCHOS O, STIASZNY B. Future generations of cathode materials: An automotive industry perspective [J]. Journal of Materials Chemistry A, 2015, 3(13): 6709−6732.

[2] HEELAN J, GRATZ E, ZHENG Zhang-feng, WANG Qiang, CHEN Meng-yuan, APELIAN D, WANG Yan. Current and prospective Li-ion battery recycling and recovery processes [J]. JOM, 2016, 68(10): 2632−2638.

[3] DONG Hong-xu, KOENIG G M. A review on synthesis and engineering of crystal precursors produced via coprecipitation for multicomponent lithium-ion battery cathode materials [J]. CrystEngComm, 2020, 22(9): 1514−1530.

[4] LI Jian, HU Le-shan, ZHOU Hong-ming, WANG Li-hua, ZHAI Bing-kun, YANG Sheng-liang, MENG Peng-yu, HU Rong. Regenerating of $LiNi_{0.5}Co_{0.2}Mn_{0.3}O_2$ cathode materials from spent lithium-ion batteries [J]. Journal of Materials Science: Materials in Electronics, 2018, 29(20): 17661−17669.

[5] LEBEDEVA N P, BOON-BRETT L. Considerations on the chemical toxicity of contemporary Li-ion battery electrolytes and their components [J]. Journal of the Electrochemical

Society, 2016, 163(6): A821−A830.

[6] ZENG Xian-lai, LI Jin-hui, LIU Li-li. Solving spent lithium-ion battery problems in China: Opportunities and challenges [J]. Renewable & Sustainable Energy Reviews, 2015, 52: 1759−1767.

[7] LI Jia, WANG Guang-xu, XU Zhen-ming. Generation and detection of metal ions and volatile organic compounds (VOCs) emissions from the pretreatment processes for recycling spent lithium-ion batteries [J]. Waste Management, 2016, 52: 221−227.

[8] BARIK S P, PRABAHARAN G, KUMAR L. Leaching and separation of Co and Mn from electrode materials of spent lithium-ion batteries using hydrochloric acid: Laboratory and pilot scale study [J]. Journal of Cleaner Production, 2017, 147: 37−43.

[9] LIU Chun-wei, LIN Jiao, CAO Hong-bin, ZHANG Yi, SUN Zhi. Recycling of spent lithium-ion batteries in view of lithium recovery: A critical review [J]. Journal of Cleaner Production, 2019, 228: 801−813.

[10] HUANG Bin, PAN Zhe-fei, SU Xiang-yu, AN Liang. Recycling of lithium-ion batteries: Recent advances and perspectives [J]. Journal of Power Sources, 2018, 399: 274−286.

[11] JIANG Feng, CHEN Yu-qian, JU Shao-hua, ZHU Qin-yu, ZHANG Li-bo, PENG Jin-hui, WANG Xu-ming, MILLER J D. Ultrasound-assisted leaching of cobalt and lithium from spent lithium-ion batteries [J]. Ultrasonics Sonochemistry, 2018, 48: 88−95.

[12] KU H, JUNG Y, JO M, PARK S, KIM S, YANG D, RHEE K, AN E M, SOHN J, KWON K. Recycling of spent lithium-ion battery cathode materials by ammoniacal leaching [J]. Journal of Hazardous Materials, 2016, 313: 138−146.

[13] LI Li, BIAN Yi-fan, ZHANG Xiao-xiao, GUAN Yi-biao, FAN Er-sha, WU Feng, CHEN Ren-jie. Process for recycling mixed-cathode materials from spent lithium-ion batteries and kinetics of leaching [J]. Waste Management, 2018, 71: 362−371.

[14] ZHANG Ze-hui, QIU Jiang-hua, YU Min, JIN Chao-zheng, YANG Bin, GUO Guang-hui. Performance of Al-doped $LiNi_{1/3}Co_{1/3}Mn_{1/3}O_2$ synthesized from spent lithium ion batteries by sol-gel method [J]. Vacuum, 2020, 172: 109105.

[15] ZHANG Rui-han, ZHENG Ya-dong, YAO Ze-yi, VANAPHUTI P, MA Xiao-tu, BONG S, CHEN Meng-yuan, LIU Yang-tao, CHENG Feng, YANG Zhen-zhen, WANG Yan. Systematic study of Al impurity for NCM622 cathode materials [J]. ACS Sustainable Chemistry & Engineering, 2020, 8(26): 9875−9884.

[16] LAI Yan-qing, YANG Jian, ZHANG Gang, TANG Yi-wei, JIANG Liang-xing, YANG Sheng-hai, LI Jie. Optimization and kinetics of leaching valuable metals from cathode materials of spent ternary lithium ion batteries with starch as reducing agent [J]. The Chinese Journal of Nonferrous Metals, 2019, 29(1): 153−160. (in Chinese)

[17] ZOU Hai-yang, GRATZ E, APELIAN D, WANG Yan. A novel method to recycle mixed cathode materials for lithium ion batteries [J]. Green Chemistry, 2013, 15(5): 1183−1191.

[18] YANG Jian, LAI Yan-qing, LIU Fang-yang, JIA Ming, JIANG Liang-xing. Countercurrent leaching of Ni, Co, Mn, and Li from spent lithium-ion batteries [J]. Waste Management & Research, 2020, 38(12): 1358−1366.

[19] JEONG M, KIM H, LEE W, AHN S J, LEE E, YOON W S. Stabilizing effects of Al-doping on Ni-rich $LiNi_{0.80}Co_{0.15}Mn_{0.05}O_2$ cathode for Li rechargeable batteries [J]. Journal of Power Sources, 2020, 474: 228592.

[20] DO S J, SANTHOSHKUMAR P, KANG S H, PRASANNA K, JO Y N, LEE C W. Al-doped $Li[Ni_{0.78}Co_{0.1}Mn_{0.1}Al_{0.02}]O_2$ for high performance of lithium ion batteries [J]. Ceramics International, 2019, 45(6): 6972−6977.

[21] YANG Xing, TANG Yi-wei, ZHENG Jian-feng, SHANG Guo-zhi, WU Jian, LAI Yan-qing, LI Jie, ZHANG Zhi-an. Tailoring structure of Ni-rich layered cathode enable robust calendar life and ultrahigh rate capability for lithium-ion batteries [J]. Electrochimica Acta, 2019, 320: 134587.

[22] YANG Xing, TANG Yi-wei, SHANG Guo-zhi, WU Jian, LAI Yan-qing, LI Jie, QU Yao-hui, ZHANG Zhi-an. Enhanced cyclability and high-rate capability of $LiNi_{0.88}Co_{0.095}Mn_{0.025}O_2$ cathodes by homogeneous Al^{3+} doping [J]. ACS Applied Materials & Interfaces, 2019, 11(35): 32015−32024.

[23] CUI Yong-fu, LIU Kun, MAN Jian-zong, CUI Jin-long, ZHANG Hai-bang, ZHAO Wen-yuan, SUN Jun-cai. Preparation of ultra-stable $Li[Ni_{0.6}Co_{0.2}Mn_{0.2}]O_2$ cathode material with a continuous hydroxide co-precipitation method [J]. Journal of Alloys and Compounds, 2019, 793: 77−85.

[24] LI Guang-yin, ZHANG Zhan-jun, WANG Ru-na, HUANG Zhen-lei, ZUO Zi-cheng, ZHOU Heng-hui. Effect of trace al surface doping on the structure, surface chemistry and low temperature performance of $LiNi_{0.5}Co_{0.2}Mn_{0.3}O_2$ cathode [J]. Electrochimica Acta, 2016, 212: 399−407.

[25] CHEN Xiang-lei, LI De, MO Yan, JIA Xiao-bo, JIA Jian-feng, YAO Chao, CHEN Da-ming, CHEN Yong. Cathode materials with cross-stack structures for suppressing intergranular cracking and high-performance lithium-ion batteries [J]. Electrochimica Acta, 2018, 261: 513−520.

[26] ZHOU Peng-fei, MENG Huan-ju, ZHANG Zhen, CHEN Cheng-cheng, LU Yan-ying, CAO Jun, CHENG Fang-yi, CHEN Jun. Stable layered Ni-rich $LiNi_{0.9}Co_{0.07}Al_{0.03}O_2$ microspheres assembled with nanoparticles as high-performance cathode materials for lithium-ion batteries [J]. Journal of Materials Chemistry A, 2017, 5(6): 2724−2731.

[27] XIANG Wei, LIU Wen-yuan, ZHANG Jun, WANG Shuo, ZHANG Ting-ting, YIN Kai, PENG Xi, JIANG Yong-chao, LIU Kai-hong, GUO Xiao-dong. Controlled synthesis of nickel-rich layered oxide cathodes with preferentially exposed {010} active facets for high rate and long cycling stable lithium-ion batteries [J]. Journal of Alloys and Compounds, 2019, 775: 72−80.

[28] YU Hai-jun, QIAN Yu-min, OTANI M, TANG Dai-ming, GUO Shao-hua, ZHU Yan-bei, ZHOU Hao-shen. Study of the lithium/nickel ions exchange in the layered $LiNi_{0.42}Mn_{0.42}Co_{0.16}O_2$ cathode material for lithium ion batteries: Experimental and first-principles calculations [J]. Energy & Environmental Science, 2014, 7(3): 1068−1078.

[29] DIXIT M, MARKOVSKY B, AURBACH D, MAJOR D T. Unraveling the effects of Al doping on the electrochemical properties of $LiNi_{0.5}Co_{0.2}Mn_{0.3}O_2$ using first principles [J].

Journal of the Electrochemical Society, 2017, 164(1): A6359−A6365.

[30] LI Ke-yan, XUE Dong-feng. Estimation of electronegativity values of elements in different valence states [J]. The Journal of Physical Chemistry A, 2006, 110(39): 11332−11337.

[31] CROGUENNEC L, BAINS J, BRÉGER J, TESSIER C, BIENSAN P, LEVASSEUR S, DELMAS C. Effect of aluminum substitution on the structure electrochemical performance and thermal stability of $Li_{1+x}(Ni_{0.40}Mn_{0.40}Co_{0.20-z}Al_z)_{1-x}O_2$ [J]. Journal of The Electrochemical Society, 2011, 158(6): A664−A670.

[32] ZHOU Fu, ZHAO Xue-mei, LU Zhong-hua, JIANG Jun-wei, DAHN J R. The effect of Al substitution on the reactivity of delithiated $LiNi_{1/3}Mn_{1/3}Co_{(1/3-z)}Al_zO_2$ with non-aqueous electrolyte [J]. Electrochemistry Communications, 2008, 10(8): 1168−1171.

[33] KIM U H, MYUNG S T, YOON C S, SUN Y K. Extending the battery life using an Al-doped $Li[Ni_{0.76}Co_{0.09}Mn_{0.15}]O_2$ cathode with concentration gradients for lithium ion batteries [J]. ACS Energy Letters, 2017, 2(8): 1848−1854.

[34] ZHAO Wen-gao, ZOU Lian-feng, JIA Hai-ping, ZHENG Jian-ming, WANG Dong-hao, SONG Jun-hua, HONG Chai-yu, LIU Rui, XU Wu, YANG Yong, XIAO Jie, WANG Chong-min, ZHANG Ji-guang. Optimized Al doping improves both interphase stability and bulk structural integrity of Ni-rich NMC cathode materials [J]. ACS Applied Energy Materials, 2020, 3(3): 3369−3377.

[35] WANG Ding, LI Xin-hai, WANG Zhi-xing, GUO Hua-jun, XU Yan, FAN Yu-lei, RU Juan-jian. Role of zirconium dopant on the structure and high voltage electrochemical performances of $LiNi_{0.5}Co_{0.2}Mn_{0.3}O_2$ cathode materials for lithium ion batteries [J]. Electrochimica Acta, 2016, 188: 48−56.

[36] NOH H J, YOUN S, YOON C S, SUN Y K. Comparison of the structural and electrochemical properties of layered $Li[Ni_xCo_yMn_z]O_2$ (x=1/3, 0.5, 0.6, 0.7, 0.8 and 0.85) cathode material for lithium-ion batteries [J]. Journal of Power Sources, 2013, 233: 121−130.

[37] JIANG Qian-qian, CHEN Ning, LIU Dong-dong, WANG Shuang-yin, ZHANG Han. Efficient plasma-enhanced method for layered $LiNi_{1/3}Co_{1/3}Mn_{1/3}O_2$ cathodes with sulfur atom-scale modification for superior-performance Li-ion batteries [J]. Nanoscale, 2016, 8(21): 11234−11240.

[38] LIU Wen, LI Xi-fei, XIONG Dong-bin, HAO You-chen, LI Jian-wei, KOU Hua-ri, YAN Bo, LI De-jun, LU Shi-gang, KOO A, ADAIR K, SUN Xue-liang. Significantly improving cycling performance of cathodes in lithium ion batteries: The effect of Al_2O_3 and $LiAlO_2$ coatings on $LiNi_{0.6}Co_{0.2}Mn_{0.2}O_2$ [J]. Nano Energy, 2018, 44: 111−120.

[39] FU Jia-le, MU Dao-bin, WU Bo-rong, BI Jia-ying, LIU Xiao-jiang, PENG Yi-yuan, LI Yi-qing, WU Feng. Enhanced electrochemical performance of $LiNi_{0.6}Co_{0.2}Mn_{0.2}O_2$ cathode at high cutoff voltage by modifying electrode/electrolyte interface with lithium metasilicate [J]. Electrochimica Acta, 2017, 246: 27−34.

[40] LI Xiang, XIE Zheng-wei, LIU Wen-jing, GE Wu-jie, WANG Hao, QU Mei-zhen. Effects of fluorine doping on structure, surface chemistry, and electrochemical performance of $LiNi_{0.8}Co_{0.15}Al_{0.05}O_2$ [J]. Electrochimica Acta, 2015, 174: 1122−1130.

[41] LU Xiao-xiao, YANG Fan, GENG Xin, XIAO Ping. Enhanced cyclability of amorphous carbon-coated SnO_2-graphene composite as anode for Li-ion batteries [J]. Electrochimica Acta, 2014, 147: 596−602.

模拟废旧锂离子电池湿法冶金浸出液再生铝掺杂 $LiNi_{0.5}Co_{0.2}Mn_{0.3}O_2$ 正极材料

李芳成[1]，张 刚[2,3]，张宗良[1]，杨 健[1]，刘芳洋[1]，贾 明[1]，蒋良兴[1]

1. 中南大学 冶金与环境学院，长沙 410083；
2. 中天超级电容器科技有限公司，南通 226463；
3. 中天新兴材料有限公司，南通 226463

摘 要：采用共沉淀法制备均相 Al 掺杂的 $LiNi_{0.5}Co_{0.2}Mn_{0.3}O_2$ 正极材料，以利用 Al 对再生镍钴锰(NCM)正极材料的正面改性作用，并改善锂离子电池回收过程中繁琐和高成本的除杂过程。当浸出液中的 Al^{3+}含量为过渡金属(Ni、Co 和 Mn)总量的 1%(摩尔分数)时，制备的 Al 掺杂 NCM 正极材料中晶格氧和 Ni^{2+}的浓度增加。在 0.1C 下的初始比容量为 167.4 mA·h/g，在 1C 下循环 400 次后容量保持率为 79.1%。此外，这种 Al 掺杂样品具有更高的倍率性能和更小的电化学阻抗。这些发现为工业上通过掺入锂离子电池回收过程中产生的 Al^{3+}杂质，重新合成具有更好电化学性能的正极材料的工艺开发提供了参考。

关键词：废旧锂离子电池；再生；铝掺杂；三元正极材料；共沉淀

(Edited by Xiang-qun LI)